Atmos. Chem. Phys., 12, 1833–1845, 2012
www.atmos-chem-phys.net/12/1833/2012/
doi:10.5194/acp-12-1833-2012

Atmospheric Chemistry and Physics

The adsorption of peroxynitric acid on ice between 230 K and 253 K

T. Ulrich[1,2], **M. Ammann**[1], **S. Leutwyler**[2], **and T. Bartels-Rausch**[1]

[1]Department of Biology and Chemistry, Paul Scherrer Institut, Villigen, Switzerland
[2]Department of Chemistry and Biochemistry, University of Berne, Berne, Switzerland

Correspondence to: T. Bartels-Rausch (thorsten.bartels-rausch@psi.ch)

Received: 12 September 2011 – Published in Atmos. Chem. Phys. Discuss.: 28 September 2011
Revised: 25 January 2012 – Accepted: 8 February 2012 – Published: 17 February 2012

Abstract. Peroxynitric acid uptake to ice and snow has been proposed to be a major loss process from the atmosphere with impacts on the atmospheric oxidation capacity. Here we present results from a laboratory study on the interaction of peroxynitric acid with water ice at low concentration. Experiments were performed in a coated wall flow tube at atmospheric pressure and in the environmentally relevant temperature range of 230 K to 253 K. The interaction was found to be fully reversible and decomposition was not observed. Analysis based on the Langmuir adsorption model showed that the partitioning of peroxynitric acid to ice is orders of magnitude lower than of nitric acid and similar to nitrous acid partitioning behavior. The partition coefficient (K_{LinC}) and its temperature dependency can be described by $3.74 \times 10^{-12} \times e^{(7098/T)}$ [cm]. Atmospheric implications are discussed and show that the uptake to cirrus clouds or to snow-packs in polar areas is an important sink for peroxynitric acid in the environment.

1 Introduction

The nitrogen oxide peroxynitric acid (HO_2NO_2) is an atmospheric trace gas that interlinks both HO_x ($= OH + HO_2$) and NO_x ($= NO + NO_2$) chemistry. Connected with those trace gas families are the rate of ozone (O_3) production and also the oxidative capacity of the atmosphere. Due to the thermal equilibrium of HO_2NO_2 with HO_2 and NO_2 (Gierczak et al., 2005), HO_2NO_2 makes up a significant fraction of the total nitrogen oxide budget mainly in the colder parts of the environment. For example, field measurements have shown gas phase concentrations of up to 3×10^{10} molecules cm^{-3} in Antarctica (Slusher et al., 2002, 2010) and 6×10^{8} molecules cm^{-3} in the upper troposphere (Kim et al., 2007). Field data further indicate a strong chemical coupling of HO_2NO_2 and NO (Davis et al., 2008; Slusher et al., 2010) and formation and deposition of HO_2NO_2 has been suggested to contribute to the reduction of OH at increasing NO levels (Grannas et al., 2007).

The fate of HO_2NO_2 in the atmosphere is not well enough known to be captured in atmospheric-chemistry models, which generally overestimate its gas-phase concentration (Slusher et al., 2002; Kim et al., 2007). Diurnal profiles of HO_2NO_2, observed at South Pole, could only be reproduced when deposition to snow was postulated as sink (Slusher et al., 2002). In the upper troposphere a HO_2NO_2 sink is also missing from the model descriptions. Currently the observed altitude profiles cannot be reproduced (Kim et al., 2007). The authors suggested uptake to ice particles in cirrus clouds as one of several potential sink processes. The choice to include a strong deposition of HO_2NO_2 to snow-packs or ice clouds is generally motivated by an earlier laboratory study that showed a significant uptake of HO_2NO_2 to ice surfaces persisting over longer times (Li et al., 1996). This result can however not be applied to atmosphere-ice interactions at environmental conditions for two reasons. First, the HO_2NO_2 concentration during the uptake experiments was up to 2×10^{13} molecules cm^{-3}. Such high levels of acidic trace gases may induce formation of hydrates and significantly alter the interaction of trace gases with the surface (Ullerstam et al., 2005; Huthwelker et al., 2006). Secondly, Li et al. (1996) identified HNO_3 as major nitrogen oxide contamination in the gas-phase with levels of up to 9 % of HO_2NO_2, which corresponds to concentrations of up to 2×10^{12} molecules cm^{-3}. In literally all of their experiments, Li et al. (1996) probed the interaction of HO_2NO_2 with nitric acid hydrates and not with water ice, which is not stable at such high HNO_3 levels (Thibert and Dominé, 1998).

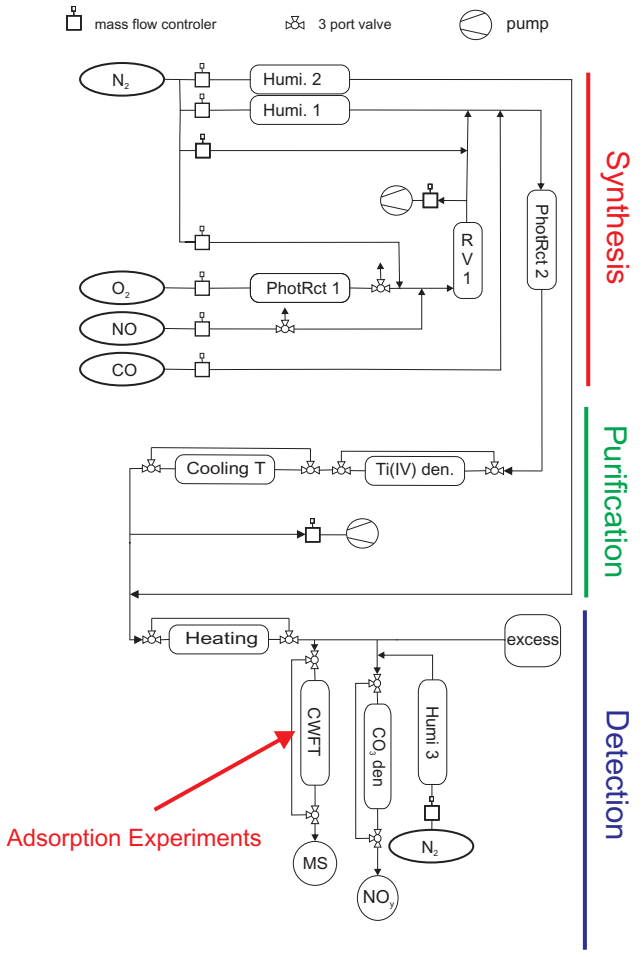

Fig. 1. Experimental setup consisting of a gas-phase synthesis, a purification step, the adsorption experiments (CWFT), and the detection step.

The main aim of this study was thus to investigate the uptake of HO_2NO_2 to ice at a low concentration of HO_2NO_2 and its by-products, where ice films are stable. A new cleaning procedure that removes by-products of the HO_2NO_2 synthesis is presented. Further, the uptake of HO_2NO_2 to ice is compared with that of other trace gases and discussed based on their solubility and acidity.

2 Methods

Figure 1 shows the setup of the experiments. First, HO_2NO_2 was synthesized in the gas phase. Then, the gas flow containing HO_2NO_2 was purified from by-products. Finally, the interaction of HO_2NO_2 with a water-ice film was studied in a coated wall flow tube (CWFT) at atmospheric pressure coupled to a chemical ionization mass spectrometer (CIMS). HO_2NO_2 and its by-products were quantified with a commercial NO_x analyzer, a commercial HONO analyzer, and a commercial H_2O_2 analyzer. In the following the experimental set-up is briefly described. Details on the synthesis of HO_2NO_2 and on the procedure to study the trace gas-ice interaction are given in the "Results and discussion" section.

2.1 Synthesis of HO_2NO_2

The synthesis has been described previously (Bartels-Rausch et al., 2011). First NO_2 is quantitatively synthesized in a reactor of 2 l (RV 1, Fig. 1) by mixing a flow of 83 ml min^{-1} NO in N_2 with a flow of 700 ml min^{-1} N_2 and with a small flow of 6 ml min^{-1} O_3 in synthetic air. O_3 is produced by irradiating dry synthetic air with 172 nm light (PhotRct 1, Fig. 1). The flow containing NO_2 is then further diluted with 700 ml min^{-1} humidified N_2, mixed with 10 ml min^{-1} CO in N_2, and irradiated in the photolysis reactor (PhotRct 2, Fig. 1). Irradiation of a $NO_2/H_2O/CO/O_2/N_2$ mixture at 172 nm yields HO_2NO_2 (Bartels-Rausch et al., 2011), see Sect. 3 for details. About half of the experiments were done at a lower CO flow of 2.5 ml min^{-1}. The residence time in the photolysis reactor was 270 ms. Relative humidity in the photolysis reactor was set to 10 %.

2.2 Purification of by-products

After the synthesis the gas flow was cleaned from by-products using a Ti(IV) oxysulfate denuder and a cooling trap at 243 K (see Sect. 3). The Ti(IV) oxysulfate denuder was prepared by wetting a 49 cm long sandblasted quartz glass tube with a inner diameter of 0.7 cm with a 5 % solution of Ti(IV) oxysulfate in 30 % H_2SO_4 (Fluka 89532) and drying the solution in a flow of N_2 until a very concentrated and highly viscous solution was obtained. The cooling trap consisted of a 46 cm long, jacketed glass tube with an inner diameter of 2.4 cm, which was filled with 10 ml quartz spheres to enhance surface area.

2.3 Coated wall flow tube

For the uptake experiments, a gas flow of typically 560 ml min^{-1} containing HO_2NO_2 was pumped from the main gas flow and passed via an ice coated flow tube (CWFT); see Sect. 3 for details on the procedure. Reynolds numbers with an average value of 112 indicate a laminar flow regime in the CWFT. To ensure water vapor equilibrium of the gas and the ice phase, the relative humidity in the gas flow was set to match the vapor pressure of the ice in the CWFT. This was done by adding 1500 ml min^{-1} N_2 that had passed a humidifier. The concentration of HO_2NO_2 in the CWFT was kept constant for all experiments.

2.4 Preparation of the ice surface

A quartz tube was etched on the inside with a 5 % solution of hydrofluoric acid (HF) in water, and then rinsed with ultra pure water (MilliQ, 0.05 µS, pH: 7.3) until the pH was

neutral. The pH was determined with a pH electrode optimized for and calibrated with solutions of low ionic strength (Orion 3 Star, Thermo). The quartz tube was then held vertically for exactly 60 s to let excess water flow out. An ice film was frozen at 258 K by rotating the quartz tube in a snuggly-fitting cooling jacket. This procedure results in smooth ice films so that its surface area can be calculated based on its geometry (Abbatt, 2003; Huthwelker et al., 2006). The total surface of the ice film was 110 cm^2. The ice had a thickness of 10 µm ± 2.7 µm as determined by weighing. The cooling jacket was tempered with a circulating ethanol bath. Temperatures were measured with a Pt100 thermo-element directly inside the CWFT at experimental conditions. The temperature gradient along the length of the flow tube was very small. At 253 K the entrance of the CWFT was about 0.03 K warmer than temperatures at its end, and at 230 K the difference was about 0.2 K. At any position temperatures were very stable; the standard deviation at 230 K was ±0.05 K.

2.5 Detection after contact with the ice

The evolution of HO_2NO_2 in the gas-phase after contact with the ice was monitored using the CIMS (Guimbaud et al., 2003). The sample gas flow of around 560 ml min^{-1} was mixed with 5 ml min^{-1} 1 % SF_6 (Messer, UHP) in Ar (Messer, 99.999 %) and 1200 ml min^{-1} N_2 (CarbaGas, 99.999 %). SF_6^- ions were produced by passing the SF_6 in N_2 through a ^{210}Po-ionizer (NRD, p-2031). HO_2NO_2 was detected with the NO_4^- (HF) cluster at *m/z* 98 (Slusher et al., 2001). With this setup detection limits (3 × standard deviation of the background signal) for HO_2NO_2 of 2.3×10^8 molecules cm^{-3} in the chemical ionization chamber were reached. This corresponds to a concentration of 5.2×10^{10} molecules cm^{-3} in the CWFT, i.e. before dilution and pressure drop.

The CIMS was further used to ensure the stability of the ice film in all experiments. We observed that the SF_6^- (H_2O) cluster at *m/z* of 164 responds strongly and reproducibly to changes in relative humidity between 0.2 % and 10 %. This cluster was continuously monitored to confirm the equilibrium of the water vapour in the gas with the ice and stable humidity in the gas flow, whether or not it passed the ice in the CWFT.

2.6 Detection of by-products before the CWFT

In a typical experiment the concentration of by-products and the performance of the two traps was monitored using the CIMS. Several clusters, which have been described earlier, have been used in this work: NO_3^- (HF) from HNO_3 at *m/z* 82 (Huey, 2007), NO_2^- (HF) from HONO and HO_2NO_2 at *m/z* 66 (Longfellow et al., 1998; Slusher et al., 2001), NO_2^- from NO_2 at *m/z* 46 (Huey, 2007) and $SF_4O_2^-$ from H_2O_2 at *m/z* 140 (Bartels-Rausch et al., 2011). The fragment with *m/z* 66 originates not only from HONO but also from HO_2NO_2. To derive HONO levels from the *m/z* 66 trace, HO_2NO_2 was thermally decomposed to establish the relative contribution of HONO and HO_2NO_2 to the *m/z* 66 trace.

2.7 Quantification

The CIMS trace of HO_2NO_2, H_2O_2 and HNO_3 was calibrated to continuously monitor their concentrations during each CWFT experiment. The concentration of the other species was determined in the gas flow after the synthesis and after the purification step, mainly to describe the performance of both steps.

In detail, the HONO concentration was quantified with a commercial HONO analyzer (LOPAP, QUMA (Heland et al., 2001; Kleffmann et al., 2002)). The H_2O_2 concentration was measured with a commercial H_2O_2 analyzer (AeroLaser AL 1002). NO, NO_2, HNO_3, and HO_2NO_2 were quantified by a commercial NO_x analyzer (Monitor Labs 9841 A). This instrument measures NO directly by chemiluminescence. In a second channel the total nitrogen oxide (NO_y) concentration is determined after conversion of those species to NO in a built-in molybdenum converter. To differentiate between the individual NO_y species, chemical traps were used (Ammann, 2001). A trap of Na_2CO_3 coated on firebricks was used to scavenge all acidic nitrogen oxides (HONO, HNO_3, and HO_2NO_2) and thus to differentiate between those and the remaining NO and NO_2 in the gas phase. Similarly, a NaCl trap was used to differentiate between HNO_3 and the other NO_y species. It consisted of a sandblasted quartz tube with a length of 49 cm and an inner diameter of 0.8 cm, that was wetted inside with a slurry of NaCl in 1/1 water/methanol and dried in a stream of N_2 (Ammann, 2001). To quantify HO_2NO_2, HO_2NO_2 was decomposed to NO_2. The Na_2CO_3 trap was then used to either scavenge HONO, HNO_3 and HO_2NO_2 or only HONO and HNO_3 (Bartels-Rausch et al., 2011). The heating unit used to decompose HO_2NO_2 was a 2 m long PFA tube (I.D.: 4 mm) heated up to 373 K with a residence time of 730 ms.

We found that the presence of CO interfered with the NO measurements. Detection of NO_y – after passage through the molybdenum converter – was not affected by CO.

2.8 Flow system

Gases originate from certified gas bottles of N_2 (Carbagas, 99.999 %), 20 % O_2 (Carbagas, 99.995 %) in N_2 (Carbagas, 99.999 %), 10 ppm NO (Messer, 99.8 %) in N_2 (Messer, 99.999 %) and 10 % CO (Messer, 99.997 %) in N_2 (Messer, 99.9999 %). Gas flows were controlled with calibrated mass flow controllers (Brooks 5850) or gas flow regulators (Voegtlin red-y) with better than 1 % accuracy. The flow through the CWFT was given by the size of the sampling orifice situated between the CWFT and the CIMS at low pressure. The volumetric gas flows were measured once a day with a gas flow calibrator (M-5 mini-Buck Calibrator,

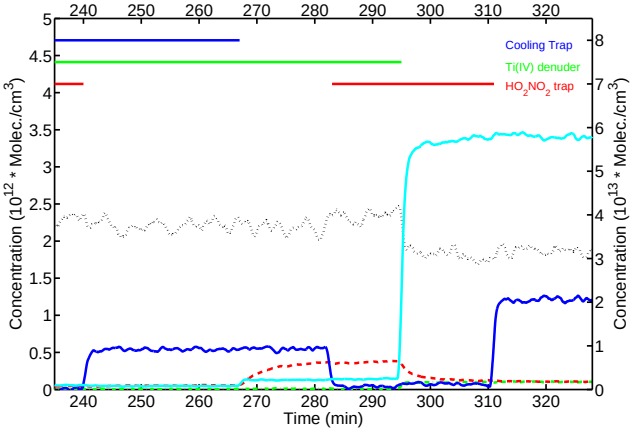

Fig. 2. Time traces of HO_2NO_2 (blue solid line, left axis) and the by-products NO_2 (black dotted line, left axis), HONO (green dash dotted line, left axis), HNO_3 (red dashed line, left axis), and H_2O_2 (turquoise solid line, right axis). Times at which traps were active are indicated by horizontal bars: Red: HO_2NO_2 trap (heating system), green: Ti(IV) denuder, blue: cooling trap. Concentrations are given without the dilution in front of the CWFT. The data were obtained at initial concentrations of 3.4×10^{12} molecules cm^{-3} NO_2, 5.4×10^{15} molecules cm^{-3} O_2, 1.6×10^{16} molecules cm^{-3} CO, and 2.36×10^{18} molecules cm^{-3} water vapor.

A.P. Buck Inc.) with 0.5 % accuracy. All flows in this work refer to standard pressure and temperature (1.013×10^5 Pa and 273.15 K). The entire flow system consisted of perfluoroalkoxy (PFA) tubing.

3 Results and discussion

3.1 Synthesis of HO_2NO_2

Conventionally HO_2NO_2 is synthesized in the aqueous phase by reaction of NO_2BF_4 in 90 % H_2O_2 or of $NaNO_2$ and $HClO_4$ in 30 % H_2O_2, which is then delivered to a gas-flow by bubbling carrier gas through the solution (Kenley et al., 1981; Appelman and Gosztola, 1995). One advantage of the gas-phase synthesis used here is that it can continuously provide HO_2NO_2 levels over long time periods, as needed for our experiments. Also, the handling of concentrated, explosive H_2O_2 solutions is omitted. Niki et al. (1977) synthesized HO_2NO_2 in the gas-phase by photolysis of HCl and subsequent reaction of the produced HO_2 with NO_2. Here, we used a different approach where H_2O is photolyzed to yield HO_2 in order to eliminate potential interference of HCl and ClONO during the adsorption experiments. We have shown previously that HO_2NO_2 yields of up to 30 % can be achieved with this synthesis route by adding CO to the photolysis gas mixture (Bartels-Rausch et al., 2011). The presence of CO reduces OH and increases HO_2 (Reactions R3 and R4) (Aschmutat et al., 2001). HO_2NO_2 is then formed by the same reaction as in the atmosphere (Niki et al., 1977):

$$HO_2 + NO_2 + M \rightarrow HO_2NO_2 + M \quad \text{(R1)}$$

The hydrolysis of water at 172 nm in the presence of oxygen is the source of HO and HO_2 (Reactions R2 and R4).

$$H_2O + h\nu \rightarrow OH + H \quad \text{(R2)}$$

$$CO + OH \rightarrow CO_2 + H \quad \text{(R3)}$$

$$H + O_2 \rightarrow HO_2 \quad \text{(R4)}$$

The main problem associated with both, gas-phase and aqueous phase, synthesis routes is the presence of by-products. HONO and HNO_3 can be formed by the reaction of NO or NO_2 with OH (Reactions R5 and R6).

$$NO_2 + OH \rightarrow HNO_3 \quad \text{(R5)}$$

$$NO + OH \rightarrow HONO \quad \text{(R6)}$$

In the absence of CO, Reaction (R5) has been used previously as a gas-phase source of HNO_3 with yields of up to 70 % (Vlasenko et al., 2009). NO was not fed into the photolysis reactor. It may presumably form during the photolysis by the reaction of NO_2 with H or with O radicals.

In this photolytic HO_2NO_2 synthesis the levels of by-products are generally rather low. HNO_3 and HONO levels of 1×10^{11} molecules cm^{-3} were determined for an initial NO_2 concentration of 3.4×10^{12} molecules cm^{-3} in the photolysis chamber (Fig. 2, 295–330 min). This is lower than observed in our previous study (Bartels-Rausch et al., 2011). The reason for this might be a more selective and direct detection mode of HNO_3 and HONO. In the previous study both species were only indirectly determined. The low levels of by-products are supported by a comparison of the rate constants showing that OH is scavenged by CO much faster than its reaction with either NO or NO_2. The ratios of rate constants of Reactions (R5)/(R3) and Reactions (R6)/(R3) are 0.06 and 0.03, respectively (Atkinson et al., 2004) and the CO concentration exceeds those of NO and NO_2 by three orders of magnitude.

Due to the interference in the chemiluminescence detection, we cannot quantify NO once CO is added to the gas flow and we can also not differentiate between NO and NO_2.

Another major by-product is H_2O_2 (Reaction R7) for which levels of up to 6×10^{13} molecules cm^{-3} have been determined in the photolysis reactor.

$$HO_2 + HO_2 \rightarrow H_2O_2 + O_2 \quad \text{(R7)}$$

3.2 Purification of the synthesis from by-products

For this study, the HO_2NO_2 synthesis was significantly improved by adding a Ti(IV) denuder to remove H_2O_2 during all experiments. Figure 2 shows the performance of the

two purification steps for a typical experimental run: Concentrations of the trace gases with time are given when the gas flow passed both the Ti(IV) denuder and the cooling trap (235–265 min), only the Ti(IV) denuder (265–295 min), and neither of the two (295–330 min). We found that the Ti(IV) denuder alone removes 96 % of the H_2O_2 (Fig. 2, 265–295 min and 295–330 min). Ti(IV) oxysulphate forms $[Ti(O_2)(OH)_{aq}]^+$ complexes with H_2O_2. This has previously been used as an analytical method (Possanzini et al., 1988). Also HONO was reduced by 94 %, and 55 % of the HO_2NO_2 is trapped by the denuder, which lowers the overall yield of the synthesis route substantially. NO_x and HNO_3 are increased by 15 % and 240 % when the Ti(IV) denuder is used. This indicates that these species were produced by redox processes in the Ti(IV) denuder system. The subsequently installed cooling trap reduces the HNO_3 concentration by 86 % and the H_2O_2 concentration by 63 % of their respective concentration after the Ti(IV) denuder (Fig. 2, 235–265 min). The remaining HNO_3 was 8 % of the HO_2NO_2 concentration, which is comparable to or lower than that reported for the two synthesis routes in the aqueous phase (Knight et al., 2002; Jimenez et al., 2004). Knight et al. (2002) measured a HNO_3 concentration of around 10 % of the HO_2NO_2 in his sample at 273 K. Jimenez et al. (2004) measured a HNO_3 concentration of around 50 % of the HO_2NO_2 concentration behind a cold trap at 252 K. Considering H_2O_2, Knight et al. (2002) measured H_2O_2 concentrations of around 50 % and Jimenez et al. (2004) of about 10 % of the HO_2NO_2 concentration, both of which are substantially lower than achieved here, even with the very efficient Ti(IV) denuder. In our experiments the H_2O_2 concentration was similar to that of HO_2NO_2.

In summary, after dilution the typical experiment resulted in a concentration of HO_2NO_2 in the CWFT of 9.7×10^{10} molecules cm^{-3} at a CO concentration of 1.6×10^{16} molecules cm^{-3}. At these conditions, the NO_2 concentration was 4×10^{11} molecules cm^{-3}, the HONO concentration was 1×10^9 molecules cm^{-3}, the HNO_3 concentration was 9×10^9 molecules cm^{-3} and the H_2O_2 concentration was 1×10^{11} molecules cm^{-3} in the CWFT.

The concentration of HO_2NO_2, H_2O_2 and HNO_3 was monitored during each individual CWFT experiment. For about half of the experiments the CO concentration was lowered to 0.4×10^{16} molecules cm^{-3} that – in qualitative agreement with our previous study – resulted in lower HO_2NO_2 yields, lower H_2O_2 yields and higher HNO_3 yields. The concentration of HO_2NO_2 was found to be very reproducible with $1.2 \times 10^{11} \pm 2.2 \times 10^{10}$ molecules cm^{-3} in the CWFT at a CO concentration of 1.6×10^{16} molecules cm^{-3} and with $8.2 \times 10^{10} \pm 1.7 \times 10^{10}$ molecules cm^{-3} at a CO concentration of 0.4×10^{16} molecules cm^{-3}. H_2O_2 concentration was $1.3 \times 10^{11} \pm 8.4 \times 10^{10}$ molecules cm^{-3} at high CO and $9.4 \times 10^{10} \pm 2.2 \times 10^{10}$ molecules cm^{-3} at low CO. HNO_3 concentration was $2 \times 10^9 \pm 1.4 \times 10^9$ molecules cm^{-3} at high CO and $7.8 \times 10^9 \pm 3.5 \times 10^9$ molecules cm^{-3} at low CO.

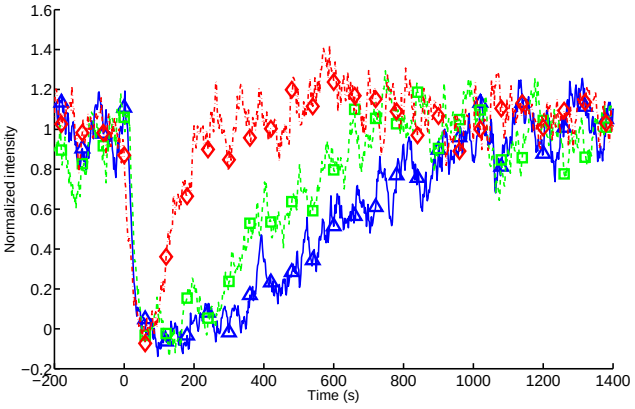

Fig. 3. Breakthrough curves of three CWFT adsorption experiments at 236 K (blue triangles), 240 K (green squares), and 250 K (red diamonds). The gas flow is led over the CWFT at time = 0 s. The variation in intensity at 250 K (t = 400–1000 s) is due to instrument fluctuations.

3.3 Adsorption experiments

Figure 3 shows typical evolutions of the HO_2NO_2 concentration with time at different temperatures as measured at the end of the CWFT. Such measurements are referred to as breakthrough curves. At time = 0 s the HO_2NO_2 in the gas flow was passed over the ice film, and its intensity drops to the background level. Then, within 200 s at our experimental conditions, the gas-phase concentration of HO_2NO_2 starts to recover. The onset of the recovery shows a temperature dependence with a longer lag-time at lower temperatures. The time needed to reach full recovery depends strongly on temperature as expected for an adsorption process. Full recovery means that the HO_2NO_2 traces recover to the average level when the CWFT was bypassed as determined before each single run, i.e. in the interval of 0 to −50 s.

The first result from this study is that HO_2NO_2 gas-phase concentration recovered to its initial level in all experiments. Incomplete recovery would suggest (i) chemical decomposition, (ii) slow, continuous uptake, or (iii) irreversible adsorption of HO_2NO_2. (i) Decomposition of HO_2NO_2 has been observed in water at moderate and acidic pH (Kenley et al., 1981; Lammel et al., 1990; Regimbal and Mozurkewich, 1997). HNO_3, NO_2, HONO, and H_2O_2 have been identified as products. Li et al. (1996) detected HNO_3 emissions from ice exposed to HO_2NO_2 and attributed those to impurities in the HO_2NO_2 source, and thus also concluded that HO_2NO_2 does not decompose on the ice surface. In our experimental setup, we would not expect to observe HNO_3 emissions from the ice, because of its strong tendency to stick to the ice surface. The CIMS traces of NO_2 at *m/z* 46 and of HONO at *m/z* 66 showed no increase when HO_2NO_2 was exposed to the ice surface, which further underlines our conclusion. (ii) HO_2NO_2 clearly does not show a long-term uptake as the HO_2NO_2 signal recovered completely within less than

Table 1. Solubility, acidity (pK_a), and adsorption enthalpies (DHads). The solubility is given as molecular Henry constant at 298 K (H_{298}).

Species	H_{298} [M/atm]				pK_a	ΔH_{ads} [kJ/mol]			
	min		max			min		max	
NO	–		–		–	-17.4	q	−22.6	q
NO_2	–		–		–	−21	q	−23	q
HONO	37	a	50	b	3.25	−32	q	−45	r
HNO_3	2.1×10^5	c	2.6×10^6	d	−1.37	−44	q	−68	s
HO_2NO_2	4×10^3	e	1.2×10^4	f	5.85	−59	t	–	
HCl	1.1	g	1.5×10^3	h	−7	–		–	
SO_2	1.1	i	1.4	j	1.77	–		–	
H_2O_2	6.9×10^4	k	1.4×10^5	l	11.6	−32	u	–	
HCOOH	9×10^2	m	1.3×10^4	n	3.7	−51	v	–	
CH_3COOH	8.3×10^2	m	1×10^4	o	4.76	−17.5	w	−55	v
CF_3COOH	8.9×10^3	p	–		0.3	–		–	

[a] Durham et al. (1981), [b] Becker et al. (1996), [c] Lelieveld and Crutzen (1991), [d] Chameides (1984), [e] Amels et al. (1996), [f] Regimbal and Mozurkewich (1997), [g] Marsh and McElroy (1985), [h] Chen et al. (1979), [i] Liss and Slater (1974), [j] Wilhelm et al. (1977), [k] Hwang and Dasgupta (1985), [l] Hoffmann and Jacob (1984), [m] Yaws and Yang (1992), [n] Servant et al. (1991), [o] Gaffney and Senum (1984), [p] Bowden et al. (1996), [q] Bartels et al. (2002), [r] Kerbrat et al. (2010b), [s] Thibert and Dominé (1998), [t] this study, [u] Pouvesle et al. (2010), [v] von Hessberg et al. (2008), [w] Sokolov and Abbatt (2002).

20 min at our experimental conditions. Table 1 lists the acidity and the molecular Henry coefficients (H_{298}) for different trace gases and shows that the observed complete recovery of HO_2NO_2 fully fits into the emerging picture where acidity largely determines the tendency for long-term uptake. The observation of a strong uptake over long timescales on thin ice films is restricted to highly acidic trace gases. Typical examples are HNO_3 (Ullerstam et al., 2005), HCl (McNeill et al., 2007), and tri-fluoroacetic acid (CF_3COOH) (Symington et al., 2010). Weaker acids, such as HO_2NO_2, show a fast and complete recovery. Analogous examples are formic acid (von Hessberg et al., 2008; Symington et al., 2010), acetic acid (Picaud et al., 2005; von Hessberg et al., 2008; Kerbrat et al., 2010a; Symington et al., 2010), HONO (Chu et al., 2000), and SO_2 (Clegg and Abbatt, 2001). The non-acidic H_2O_2 shows no long term uptake (Clegg and Abbatt, 2001; Pouvesle et al., 2010). For the weak acids HONO and SO_2 a long term uptake has been observed in packed bed flow tubes that have a much larger ice volume and surface area and are thus much more sensitive to slow bulk and surface effects (Huthwelker et al., 2001; Kerbrat et al., 2010b). Molecular solubility seems not to be a strong driver for long-term uptake (Table 1). Instrumental fluctuations of ±5 % however give the possibility that small deviations from the complete recovery remained undetected in our experiments. (iii) To test the reversibility of the uptake, the number of desorbing molecules was determined in 4 experiments at 230, 236, 238 and 244 K, respectively. This was done by exposing the ice to HO_2NO_2 until the adsorption equilibrium was reached, thermally decomposing HO_2NO_2 to NO_2 and HO_2 in the gas flow entering the CWFT, and monitoring the HO_2NO_2 release from the ice. The number of adsorbed and desorbed molecules was equal within the uncertainty of the measurements (±50 %) for the individual experiments below 240 K, indicating fully reversible uptake. At 244 K, the number of desorbed molecules was lower than the number of adsorbed molecules. This might in principle be due to altered surface characteristics of the ice at higher temperatures. However, since also results from the preceding adsorption experiment did lie outside the confidence interval of the data set, we concluded that this measurement is an outlier and do not consider it any further. The observation of reversible adsorption is in agreement with other data available for weak acids or non-acidic species such as H_2O_2 (Pouvesle et al., 2010), acetone (Winkler et al., 2002; Peybernes et al., 2004; Bartels-Rausch et al., 2005), formic acid (von Hessberg et al., 2008) and acetic acid (Sokolov and Abbatt, 2002; Symington et al., 2010). For the strong acids HNO_3 (Ullerstam et al., 2005) and HCl (McNeill et al., 2006) the peak area was significantly lower in the desorption experiments, showing that the adsorption was not reversible for these strong acids.

In summary, the uptake of HO_2NO_2 to the ice surface can be described as reversible adsorption equilibrium at temperatures from 230 K to 253 K.

3.4 Partition coefficient

3.4.1 Surface coverage

The number of adsorbed HO_2NO_2 molecules (n_{ads}) in equilibrium is the primary observable of these experiments and is directly derived from the breakthrough curve:

$$n_{ads} = F(T) \cdot \text{Int\_Area} \cdot \frac{p_{HO_2NO_2} \cdot N_a}{R \cdot T} \quad (1)$$

Here, $F(T)$ is the volumetric velocity of the gas flow in $cm^3\,s^{-1}$ at T [K] – the temperature of the CWFT, Int_Area

is the integrated area of the curve in s, p_{HO2NO2} is the partial pressure of HO_2NO_2 [MPa], N_a is the Avogadro constant [molecules mol^{-1}], R is the universal gas constant [J mol^{-1} K^{-1}]. The surface concentration of adsorbed HO_2NO_2 molecules at our experimental conditions ranged from $6.1^{+2.8}_{-2.3} \times 10^{11}$ molecules cm^{-2} at 253 K to $7.7^{+4.4}_{-2.5} \times 10^{12}$ molecules cm^{-2} HO_2NO_2 at 230 K. All uncertainties are given as 95 % confidence interval. Surface coverage is at most a few percent of a monolayer, as estimated with a maximal monolayer capacity of 3×10^{14} molecules cm^{-2} found for HONO and HNO_3 (Crowley et al., 2010). Adsorption at such a low surface coverage is most likely in the linear adsorption regime of the Langmuir adsorption isotherm.

To compare the adsorption behavior among different trace gases we express the adsorption equilibrium in terms of the partition coefficient K_{LinC} (cm), which is defined as ratio of the concentration of adsorbed molecules to the gas-phase concentration at equilibrium and which describes the initial linear part of an adsorption isotherm as defined by the Langmuir model. At equilibrium the surface concentration of adsorbates is related to the gas-phase concentration as:

$$K_{LinC} = \frac{\frac{n_{ads}}{A}}{\frac{n_{gas}}{V}}, \quad (2)$$

where n_{gas} is the number of molecules in the gas phase [molecules], n_{ads} is the number of molecules adsorbed on the ice [molecules], V the volume of the flow tube [cm^3] and A the geometric surface area of the ice film [cm^2]. The Langmuir model has proven to describe the partitioning of a number of atmospheric trace gases well, including HNO_3 at low coverage (Ullerstam et al., 2005), HONO (Kerbrat et al., 2010b) and VOCs (Sokolov and Abbatt, 2002) and has also been adopted by IUPAC (Crowley et al., 2010).

Figure 4 shows the natural logarithm of K_{LinC}, plotted versus the inverse temperature in the temperature range of 230 K to 253 K. K_{LinC} at 230 K is 94.4^{+49}_{-32} cm and decreases to $5.7^{+3.0}_{-2.0}$ cm at 253 K. The logarithmic data follow a linear trend, clearly showing that reversible partitioning describes the interaction of HO_2NO_2 with the ice surface very well. The linear fit of $\ln(K_{LinC})$ vs. $1/T$ allows to describe the temperature dependency of K_{LinC} as $3.74 \times 10^{-12} \times e^{(7098/T)}$; the uncertainty of the exponent is ±661 K. Such a negative Arrhenius type temperature dependency is in agreement with other trace gases that physically adsorb on ice (Huthwelker et al., 2006). Figure 4 also shows that K_{LinC} of HO_2NO_2 is nearly three orders of magnitude lower than the K_{LinC} of HNO_3 and lies in the same range as the K_{LinC} of HONO over the temperature range investigated. This means that at equilibrium HO_2NO_2 adsorbs less to ice than HNO_3 and about as much as HONO. The K_{LinC} values for HNO_3 and HONO were taken from the recent IUPAC compilation (Crowley et al., 2010) and are based on the following work: Abbatt (1997), Chu et al. (2000), Cox et al. (2005), Hynes et al. (2002), Kerbrat et al. (2010b), and Ullerstam et al. (2005).

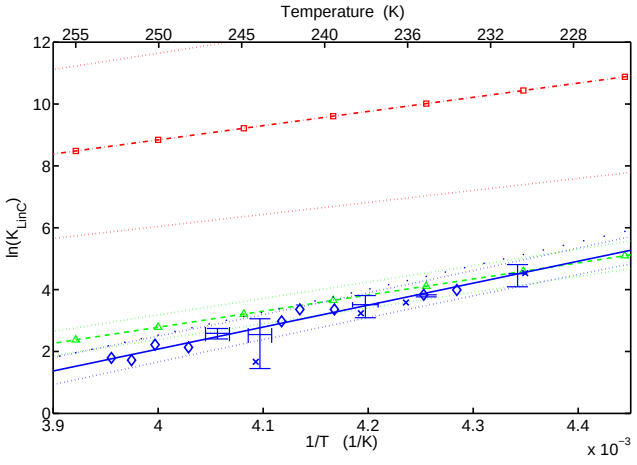

Fig. 4. Natural logarithm of K_{LinC} versus the inverse temperature for HO_2NO_2 (blue diamonds). When several data points were available mean values are plotted with an uncertainty of two times the standard deviation. The blue, dotted lines give the 95 % confidence bounds for the linear fit (blue solid line). The thick blue dots give the maximum error with included competitive adsorption. The blue crosses indicate desorption experiments. The data are compared to the IUPAC recommendation (Crowley et al., 2010) for HONO (green, dashed line with triangles) and HNO_3 (red, dash-dotted line with squares). The dotted lines show the error for HONO and HNO_3 according to the IUPAC recommendation.

This relative adsorption strength is in agreement with our previous study, where the migration of HO_2NO_2, HNO_3, HONO, and NO_2 was investigated in a flow tube packed with ice along which temperature decreased with distance (Bartels-Rausch et al., 2011). Those experiments showed an increasing preference for the ice phase in the sequence $NO_2 < HONO = HO_2NO_2 < HNO_3$. It is also in agreement with Li et al. (1996) who observed that HNO_3 desorbs at higher temperatures (246 K) than HO_2NO_2 (225 K) in temperature programmed desorption experiments.

3.4.2 Influence of solubility on the adsorption process

This relative order of K_{LinC} apparently scales with the effective solubility of the individual species in water (Table 1 and Fig. 5). Figure 5 shows the results of a multiple linear regression between the partitioning to ice, the acidity constant, and the molecular Henry constant for SO_2, HCOOH, CH_3COOH, CF_3COOH, HONO, HNO_3, HO_2NO_2, HCl and H_2O_2. The correlation is rather good when considering the large errors that might be associated with the three input parameters. Especially, the reported values of H_{298} for HO_2NO_2 might be overestimated as HO_2NO_2 easily decomposes in water, which makes reliable measurement of H_{298} difficult.

The good correlation illustrates the importance of both the acidity and the solubility on the partitioning to ice. Apparently similar molecular properties determine the tendency for

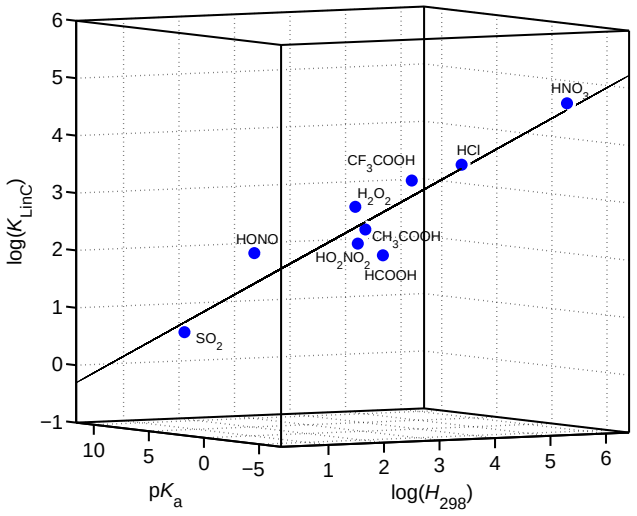

Fig. 5. Multiple linear regression with the input parameters acid dissociation constant (pK_a) and molecular Henry constant (H_{298} [M atm^{-1}]) versus the K_{LinC} [cm^{-1}] on ice at 228 K.

uptake into water and the adsorption on ice for these acidic trace gases. This even holds for acidic organic trace gases. The relationship found is given in Eq. (4) and can be used to roughly estimate the partitioning of any acidic trace gas to ice.

$$\log(K_{LinC}) = 0.4977 \cdot \log(H_{298}) - 0.1282 \cdot pK_a + 1.1362. \quad (3)$$

3.5 Enthalpy of adsorption

The slope of the linear fits to the data in the $\ln(K_{LinC})$ versus the inverse temperature plot (Fig. 4) is steeper for HO_2NO_2 than for HNO_3 or HONO. This impression is confirmed by a statistical F-test, which compares the slopes of the regressions in a pairwise manner based on the standard deviation of each. The slope and standard deviation for HNO_3 and for HONO were derived from the IUPAC recommendation (Crowley et al., 2010). From the slope the standard enthalpy of adsorption (ΔH^0_{ads}) of $-59.0 \pm 5.5\,kJ \times mol^{-1}$ can be derived for HO_2NO_2. When comparing ΔH^0_{ads} with literature values for other nitrogen oxides as given in Table 1, one obtains the sequence $NO < NO_2 < HONO = HNO_3 < HO_2NO_2$. The very high enthalpy of adsorption for HNO_3 reported by Thibert and Dominé (1998) of $-68 \pm 8.9\,kJ\,mol^{-1}$ was not considered. The higher enthalpy of adsorption compared to the other nitrogen oxides indicates stronger HO_2NO_2-ice interactions.

4 Effect of by-products

Despite careful purification steps, there is a possibility that the remaining H_2O_2, HNO_3, HONO, NO_2, and NO can interfere with the adsorption measurements of HO_2NO_2 and this is discussed below. NO and NO_2 do not interact with the ice at temperatures of our experiment (Bartels et al., 2002), thus their presence does not influence the adsorption measurements of HO_2NO_2. Dimerization of NO_2 to N_2O_4 is unlikely at these low concentrations and is thus neglected. HONO does adsorb to the ice, but since its concentration is only 1 % of HO_2NO_2 its contribution can be neglected. HNO_3 and H_2O_2 are present at relatively high concentration and both partition to ice surfaces. We monitored their gas phase concentration after the CWFT with the CIMS during each experiment. In all experiments the HNO_3 signal remained at background level, while the onset of the recovery for the H_2O_2 signal was only visible in longer experiments (around 45 min). This observation strongly suggests larger partitioning of either species to ice compared to HO_2NO_2. This is consistent with the work on H_2O_2 adsorption to ice by Pouvesle et al. (2010). An earlier work has shown much weaker partitioning to the ice (Clegg and Abbatt, 2001).

To estimate the impact of HNO_3 and H_2O_2 on HO_2NO_2 adsorption, the length on which they are present in the CWFT was derived. For this the surface coverage (Eq. 2) was calculated with K_{LinC} taken from Crowley et al. (2010) and Pouvesle et al. (2010) and with the measured gas phase concentration. The total area, i.e. the length, in the column where both species adsorb is then derived based on the total flux of molecules into the CWFT during the experiment and the surface coverage. HNO_3 completely adsorbs within less than 2 cm of the flow tube at any temperature and its influence on the partitioning of HO_2NO_2 to the ice in equilibrium over the whole length of the CWFT is thus neglected. H_2O_2 adsorbs along a length of up to 30 cm with a surface coverage ranging from 5 % to 10 % in the temperature range of 253 K to 238 K, and from 10 % to 18 % below 238 K. Such a high surface coverage of an additional trace gas during uptake experiments might lead to a reduction in adsorbed HO_2NO_2 molecules, because both species compete for adsorption sites on the ice. To quantify the possible influence of H_2O_2 on the adsorption of HO_2NO_2, we used the competitive Langmuir model as detailed in Kerbrat et al. (2010a). The model showed that K_{LinC} is reduced by 20 % at 230 K, by 8 % at 238 K and by 5 % at 250 K. This is thus a potential systematic error of our results at low temperatures. However, as the deviation is well within the experimental scatter of K_{LinC}, we neglected the influence of competitive adsorption (Fig. 4).

All experiments were done in the ice stability regime of the HNO_3-water phase diagram (Thibert and Dominé, 1998), and the H_2O_2-water phase diagram (Foley and Giguere, 1951). Yet, surface modification of the ice by HNO_3 could be important along the first 2 cm of the CWFT. McNeill et al. (2006) have observed increased adsorption of acetic acid to ice when another strong acid, HCl, was dosed to the surface at a concentration that induced surface premelting. McNeill et al. (2006) observed this increased adsorption at HCl concentrations near the boundary of the solid ice stability regime of the HCl-water phase diagram. For partial pressures

corresponding more to the center of the ice stability regime in the phase diagram no premelting and no increased uptake of acetic acid was observed. The HNO_3 concentration in this study was rather in the middle of the solid ice stability regime of the HNO_3-water phase diagram, making it unlikely that surface modifications might have occurred which enhance the uptake of HO_2NO_2. In agreement, solid ice was still observed at the surface in presence of nitrate at concentrations similar to this study (Krepelova et al., 2010).

The presence of by-products, esp. H_2O_2, might have altered the adsorption of HO_2NO_2. However, this effect is not larger than the random fluctuations of our results. We thus do not correct our values for systematic error and think that the results given here are a good representation of environmentally relevant conditions.

5 Uncertainties

The uncertainty of n_{ads}, K_{LinC}, the exponent of the Arrhenius temperature dependency, and of ΔH^0_{ads} was determined by the 95 % confidence interval of the fit through 22 data points. The reported error represents random variations between individual experiments and is expressed as 2 times the standard deviation in each direction. The 95 % confidence interval of the fit agreed well with the confidence interval of 5 repeated experiments at 230 K. A rough estimation of the individual contributions to the total uncertainty revealed that fluctuations in n_{ads}, which are 19 % of the mean value and instrumental fluctuations, which are 5 % of the mean value, contribute strongly to the uncertainty of n_{ads}. Other random fluctuations like the temperature of the CWFT or the fluctuations of the flow through the CWFT have a lower impact on the error.

Co-adsorption has been discussed as a source of systematic error in the determination of K_{LinC} of HO_2NO_2 and it was found that this negligible (Sect. 4). This conclusion relies on calculations based on $n_{max}(H_2O_2)$, $n_{max}(HO_2NO_2)$, the gas phase concentration of H_2O_2, and $K_{LinC}(H_2O_2)$. Each of these parameters has an uncertainty by itself. The effect on $K_{LinC}(HO_2NO_2)$ of each is discussed in the following. An error in n_{max} of H_2O_2 and of HO_2NO_2 was found to be negligible. In the interval of n_{max} from 2×10^{14} molecules cm^{-2} to 4×10^{14} molecules cm^{-2}, K_{LinC} only changed by 7 % at 230 K. The gas phase concentration of H_2O_2, which was tested in the ±50 % interval, changed K_{LinC} by 7 % at 230 K. This is also within the experimental scatter. A change in K_{LinC} of H_2O_2 within a +150 %–66 % interval, leads to a change in K_{LinC} of 22 %. This effect was the greatest, but still inside the bounds of error of experimental scatter. In summary the conclusion, that co-adsorption is negligible, is valid even when considering the systematic uncertainty.

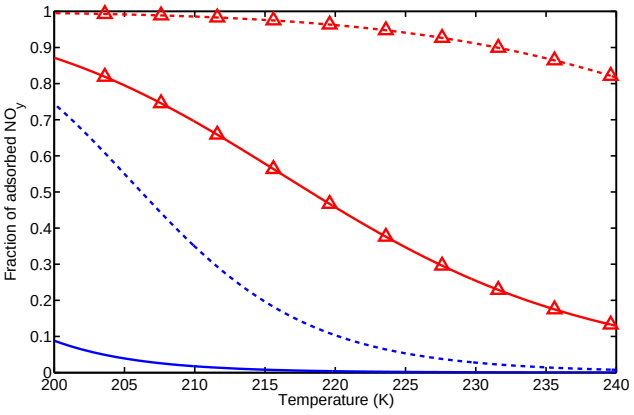

Fig. 6. Fraction of adsorbed HO_2NO_2 (blue line) and HNO_3 (red line, triangles) to cirrus clouds at temperatures of the upper troposphere. Solid lines represent clouds with a surface area density of 10^{-5} cm^{-1}, dashed lines represent clouds with a surface area density of 3×10^{-4} cm^{-1}. Data for HNO_3 was taken from the IUPAC recommendations (Crowley et al., 2010), the data for HO_2NO_2 is from this work.

6 Atmospheric implications

Ice surfaces have been proposed to represent a sink for gas phase HO_2NO_2 (Slusher et al., 2002; Kim et al., 2007), and the magnitude of the uptake of HO_2NO_2 to ice surfaces has been proposed to be similar to that of HNO_3 (Slusher et al., 2002). In this study we show that equilibrium partitioning of HO_2NO_2 to ice at low concentration is orders of magnitude lower than expected purely based on its molecular solubility. Molecular Henry constants have been used to estimate the gas phase concentration of HO_2NO_2 over ice surfaces (Abida et al., 2011). Here we discuss the equilibrium partitioning of HO_2NO_2 to ice clouds in the upper troposphere and to surface snow-packs under environmentally relevant conditions once the adsorption equilibrium is reached.

Figure 6 shows the fraction of HO_2NO_2 adsorbed to the ice phase in typical cirrus clouds in the upper troposphere. Typical temperatures and surface area densities of dense cirrus clouds, 3×10^{-4} to 10^{-5} cm^2 ice surface per cm^3 of free gas phase, were taken from observations (Popp et al., 2004). The temperatures for the experiments presented in this work range from 230 K to 253 K. Data is extrapolated to temperatures down to 200 K in Fig. 6 which potentially adds uncertainty. Taken the excellent linear fit of $\ln(K_{LinC})$ to 1/T that represents our data, we suggest that this extrapolation is reasonable for a rough estimate of the partitioning of HO_2NO_2 to ice in the upper troposphere. The fraction of the adsorbed nitrogen oxides was calculated as proposed by Pouvesle et al. (2010):

$$\alpha = \frac{K_{LinC}\cdot SAD}{K_{LinC}\cdot SAD + 1}, \quad (4)$$

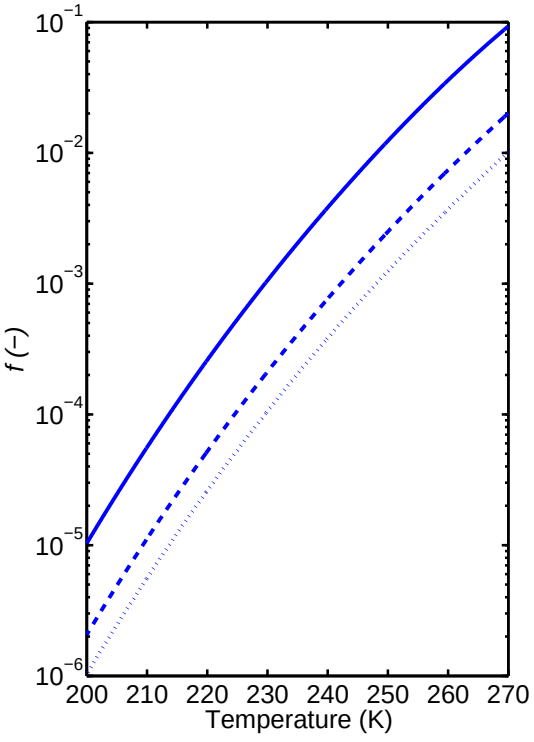

Fig. 7. Retention factor f versus temperature for three different surface area densities of snow: Solid line = 10 cm^{-1}, dashed line: 50 cm^{-1} and dotted line: 100 cm^{-1}.

where α [–] is the adsorbed fraction, K_{LinC} [cm] the partition coefficient as a function of the temperature and SAD [cm^{-1}] is the ice surface area per volume of gas phase (surface area density). The adsorption of HO_2NO_2 to the ice particles is only significant at cold temperatures (<210 K) and very dense cirrus clouds (3×10^{-4} cm^{-1}); then up to 70 % of the total HO_2NO_2 is trapped. Thus when very dense clouds are present the equilibrium partitioning of HO_2NO_2 to cirrus clouds could explain the discrepancy between measured and modeled data for HO_2NO_2 in the upper troposphere.

Considering the snow cover on the ground, the surface area to air-volume ratio is orders of magnitude higher than in clouds (see below) and HO_2NO_2 adsorbs almost completely to the ice phase in the interstitial air of snow even at warmer temperatures. The specific surface area ranges from 20 cm^2 g^{-1} to >1000 cm^2 g^{-1} for melt-freeze crust and fresh dentritic snow, respectively. The density and solid to air volume ratio ranges from 0.1 g cm^{-3} to 0.6 g cm^{-3} for fresh and wind-packed snow, respectively (Dominé et al., 2008). The resulting surface area densities are in the range of 10s to 100s cm^{-1}. This extensive partitioning to the ice phase directly influences the transport of HO_2NO_2 through a snow-pack by diffusion. The diffusivity of species with a strong tendency to stick to ice surfaces, i.e. large K_{LinC}, is attenuated by a factor $1/f$ (Eq. 8).

$$f_{HO_2NO_2} = \frac{1}{1 + SAD \cdot K_{LinC,HO_2NO_2}} \quad (5)$$

Figure 7 shows f versus the temperature typical for snow-covered environments for a range of surface area densities, where the high SAD value represents fresh dentritic snow and the low value wind packed snow. At temperatures below 240 K diffusion is slowed by more than hundred times due to the interaction with the ice surface for any given snow-pack.

In summary snow and ice particles represent a sink for HO_2NO_2 in the environment. The snow pack represents a sink at any typical temperature; adsorption of HO_2NO_2 on atmospheric ice particles strongly depends on the density of the ice clouds and temperature.

7 Conclusions

The adsorption of HO_2NO_2 on ice and its temperature dependence has been characterized at low surface coverage. At our experimental conditions, uptake of HO_2NO_2 to ice is fully reversible and a slow, long-term loss to the ice was not observed. The partition constant K_{LinC} with a negative temperature dependence of $3.74 \times 10^{-12} \times e^{(7098/T)}$ (cm) was derived. Partitioning to ice of HO_2NO_2 is orders of magnitude smaller than values for HNO_3, and in the same range as values reported for HONO. Acidity and solubility of acidic trace gases could have an important impact on the adsorption behavior. Cirrus clouds in the upper troposphere and ice and snow surfaces at South Pole and other very cold parts of the environment are a sink for gas-phase HO_2NO_2.

Acknowledgements. We gratefully thank M. Birrer for excellent technical support. We thank Josef Dommen and Peter Mertes for providing and help with the H_2O_2 analyzer. We also thank Yulia Sosedova for help with the HONO analyzer. We thank I. Zimmermann and J. Graell for their work on this project during their internships with us. We appreciate funding by the Swiss National Science Foundation, grant number 200021_121857.

Edited by: V. F. McNeill

References

Abbatt, J. P. D.: Interaction of HNO_3 with water-ice surfaces at temperatures of the free troposphere, Geophys. Res. Lett., 24, 1479–1482, doi:10.1029/97GL01403, 1997.

Abbatt, J. P. D.: Interactions of atmospheric trace gases with ice surfaces: Adsorption and reaction, Chem. Rev., 103, 4783–4800, doi:10.1021/cr0206418, 2003.

Abida, O., Mielke, L. H., and Osthoff, H. D.: Observation of gas-phase peroxynitrous and peroxynitric acid during the photolysis of nitrate in acidified frozen solutions, Chem. Phys. Lett., 511, 187–192, doi:10.1016/j.cplett.2011.06.055, 2011.

Amels, P., Elias, H., Götz, U., Steingens, U., and Wannowius, K. J.: Chapter 3.1: Kinetic investigation of the stability of peroxonitric acid and of its reaction with sulfur(IV) in aqueous solution, edited by: Warneck, P., Springer Verlag, Berlin, 77–88 pp., 1996.

Ammann, M.: Using N-13 as tracer in heterogeneous atmospheric chemistry experiments, Radiochim. Acta, 89, 831–838, doi:10.1524/ract.2001.89.11-12.831, 2001.

Appelman, E. H. and Gosztola, D. J.: Aqueous peroxynitric acid ($HOONO_2$) – a novel synthesis and some chemical and spectroscopic properties, Inorg. Chem., 34, 787–791, doi:10.1021/ic00108a007, 1995.

Aschmutat, U., Hessling, M., Holland, F., and Hofzumahaus, A.: A tunable source of hydroxyl (OH) and hydroperoxy (HO_2) radicals: in the range between 10^6 and 10^9 cm^{-3}, Institut für Atmosphärische Chemie, Forschungszentrum Jülich, Jülich, 811–816, 2001.

Atkinson, R., Baulch, D. L., Cox, R. A., Crowley, J. N., Hampson, R. F., Hynes, R. G., Jenkin, M. E., Rossi, M. J., and Troe, J.: Evaluated kinetic and photochemical data for atmospheric chemistry: Volume I – gas phase reactions of O_x, HO_x, NO_x and SO_x species, Atmos. Chem. Phys., 4, 1461–1738, doi:10.5194/acp-4-1461-2004, 2004.

Bartels, T., Eichler, B., Zimmermann, P., Gäggeler, H. W., and Ammann, M.: The adsorption of nitrogen oxides on crystalline ice, Atmos. Chem. Phys., 2, 235–247, doi:10.5194/acp-2-235-2002, 2002.

Bartels-Rausch, T., Huthwelker, T., Gaggeler, H. W., and Ammann, M.: Atmospheric pressure coated-wall flow-tube study of acetone adsorption on ice, J. Phys. Chem. A, 109, 4531–4539, 2005.

Bartels-Rausch, T., Ulrich, T., Huthwelker, T., and Ammann, M.: A novel synthesis of the radiactively labelled atmospheric trace gas peroxynitirc acid, Radiochim. Acta, 99, 1–8, doi:10.1524/ract.2011.1830, 2011.

Becker, K. H., Kleffmann, J., Kurtenbach, R., and Wiesen, P.: Solubility of nitrous acid (HONO) in sulfuric acid solutions, J. Phys. Chem.-US, 100, 14984–14990, doi:10.1021/jp961140r, 1996.

Bowden, D. J., Clegg, S. L., and Brimblecombe, P.: The Henry's law constant of trifluoroacetic acid and its partitioning into liquid water in the atmosphere, Chemosphere, 32, 405–420, doi:10.1016/0045-6535(95)00330-4, 1996.

Chameides, W. L.: The photochemistry of a remote marine stratiform cloud, J. Geophys. Res.-Atmos., 89, 4739–4755, 10.1029/JD090iD03p05865, 1984.

Chen, C. C., Britt, H. I., Boston, J. F., and Evans, L. B.: Extension and Application of the Pitzer Equation for Vapor-Liquid-Equilibrium of Aqueous-Electrolyte Systems with Molecular Solutes, Aiche Journal, 25, 820–831, doi:10.1002/aic.690250510, 1979.

Chu, L., Diao, G. W., and Chu, L. T.: Heterogeneous interaction and reaction of HONO on ice films between 173 and 230 K, J. Phys. Chem. A, 104, 3150–3158, doi:10.1021/jp9937151, 2000.

Clegg, S. M. and Abbatt, J. P. D.: Uptake of gas-phase SO_2 and H_2O_2 by ice surfaces: Dependence on partial pressure, temperature, and surface acidity, J. Phys. Chem. A, 105, 6630–6636, doi:10.1021/jp010062r, 2001.

Cox, R. A., Fernandez, M. A., Symington, A., Ullerstam, M., and Abbatt, J. P. D.: A kinetic model for uptake of HNO_3 and HCl on ice in a coated wall flow system, Phys. Chem. Chem. Phys., 7, 3434–3442, doi:10.1039/b506683b, 2005.

Crowley, J. N., Ammann, M., Cox, R. A., Hynes, R. G., Jenkin, M. E., Mellouki, A., Rossi, M. J., Troe, J., and Wallington, T. J.: Evaluated kinetic and photochemical data for atmospheric chemistry: Volume V – heterogeneous reactions on solid substrates, Atmos. Chem. Phys., 10, 9059–9223, doi:10.5194/acp-10-9059-2010, 2010.

Davis, D. D., Seelig, J., Huey, G., Crawford, J., Chen, G., Wang, Y., Buhr, M., Helmig, D., Neff, W., Blake, D., Arimoto, R., and Eisele, F.: A reassessment of Antarctic plateau reactive nitrogen based on ANTO 2003 airborne and ground based measurements, Atmos. Envrion., 42, 2831–2848, doi:10.1016/j.atmosenv.2007.07.039, 2008.

Dominé, F., Albert, M., Huthwelker, T., Jacobi, H.-W., Kokhanovsky, A. A., Lehning, M., Picard, G., and Simpson, W. R.: Snow physics as relevant to snow photochemistry, Atmos. Chem. Phys., 8, 171–208, doi:10.5194/acp-8-171-2008, 2008.

Durham, J. L., Overton, J. H., and Aneja, V. P.: Influence of gaseous nitric-acid on sulfate production and acidity in rain, Atmos. Envrion., 15, 1059–1068, doi:10.1016/0004-6981(81)90106-2, 1981.

Foley, W. T. and Giguere, P. A.: Hydrogen peroxide and its analogues. 2. Phase equilibrium in the system hydrogen peroxide water, Canadian Journal of Chemistry-Revue Canadienne De Chimie, 29, 123–132, doi:10.1139/v51-016, 1951.

Gaffney, J. S. and Senum, G. I.: presented at the Conference on Gas-Liquid Chemistry of Natural Waters, Brookhaven National Laboratory, April 1984, Paper No. 5, BNL 51757, Vol. 1, 1984.

Gierczak, T., Jimenez, E., Riffault, V., Burkholder, J. B., and Ravishankara, A. R.: Thermal decomposition of HO_2NO_2 (peroxynitric acid, PNA): Rate coefficient and determination of the enthalpy of formation, J. Phys. Chem. A, 109, 586–596, doi:10.1021/jp046632f, 2005.

Grannas, A. M., Jones, A. E., Dibb, J., Ammann, M., Anastasio, C., Beine, H. J., Bergin, M., Bottenheim, J., Boxe, C. S., Carver, G., Chen, G., Crawford, J. H., Dominé, F., Frey, M. M., Guzmán, M. I., Heard, D. E., Helmig, D., Hoffmann, M. R., Honrath, R. E., Huey, L. G., Hutterli, M., Jacobi, H. W., Kln, P., Lefer, B., McConnell, J., Plane, J., Sander, R., Savarino, J., Shepson, P. B., Simpson, W. R., Sodeau, J. R., von Glasow, R., Weller, R., Wolff, E. W., and Zhu, T.: An overview of snow photochemistry: evidence, mechanisms and impacts, Atmos. Chem. Phys., 7, 4329–4373, doi:10.5194/acp-7-4329-2007, 2007.

Guimbaud, C., Bartels-Rausch, T., and Ammann, M.: An atmospheric pressure chemical ionization mass spectrometer (APCI-MS) combined with a chromatographic technique to measure the adsorption enthalpy of acetone on ice, Int. J. Mass. Spectrom., 226, 279–290, doi:10.1016/S1387-3806(03)00019-8, 2003.

Heland, J., Kleffmann, J., Kurtenbach, R., and Wiesen, P.: A new instrument to measure gaseous nitrous acid (HONO) in the atmosphere, Environ. Sci. Technol., 35, 3207–3212, doi:10.1021/es000303t, 2001.

Hoffmann, M. R. and Jacob, D. J.: Kinetics and mechanisms of the catalytic oxidation of dissolved sulfur dioxide in aqueous solution: An application to nighttime fog water chemistry, in: SO_2, NO and NO_2 oxidation mechanisms: Atmospheric considerations, edited by: Calvert, J. G., Butterworth Publishers, Bosten, MA, 101–172, 1984.

Huey, L. G.: Measurement of trace atmospheric species by chemical ionization mass spectrometry: Speciation of reactive nitrogen and future directions, Mass. Spectrom. Rev., 26, 166–184, doi:10.1002/mas.20118, 2007.

Huthwelker, T., Lamb, D., Baker, M., Swanson, B., and Peter, T.: Uptake of SO_2 by polycrystalline water ice, J. Colloid Interf.

Sci., 238, 147–159, doi:10.1006/jcis.2001.7507, 2001.

Huthwelker, T., Ammann, M., and Peter, T.: The uptake of acidic gases on ice, Chem. Rev., 106, 1375–1444, doi:10.1021/cr020506v, 2006.

Hwang, H. and Dasgupta, P. K.: Thermodynamics of the hydrogen-peroxide water-system, Environ. Sci. Technol., 19, 255–258, doi:10.1021/es00133a006, 1985.

Hynes, R. G., Fernandez, M. A., and Cox, R. A.: Uptake of HNO_3 on water-ice and coadsorption of HNO_3 and HCl in the temperature range 210–235 K, J. Geophys. Res.-Atmos., 107, 4797, doi:10.1029/2001JD001557, 2002.

Jimenez, E., Gierczak, T., Stark, H., Burkholder, J. B., and Ravishankara, A. R.: Reaction of OH with HO_2NO_2 (peroxynitric acid): Rate coefficients between 218 and 335 K and product yields at 298 K, J. Phys. Chem. A, 108, 1139–1149, doi:10.1021/jp0363489, 2004.

Kenley, R. A., Trevor, P. L., and Lan, B. Y.: Preparation and thermal-decomposition of pernitric acid ($HOONO_2$) in aqueous-media, J. Am. Chem. Soc., 103, 2203–2206, doi:10.1021/ja00399a012, 1981.

Kerbrat, M., Huthwelker, T., Bartels-Rausch, T., Gäggeler, H. W., and Ammann, M.: Co-adsorption of acetic acid and nitrous acid on ice, Phys. Chem. Chem. Phys., 12, 7194–7202, doi:10.1039/b924782c, 2010a.

Kerbrat, M., Huthwelker, T., Gäggeler, H. W., and Ammann, M.: Interaction of nitrous acid with polycrystalline ice: Adsorption on the surface and diffusion into the bulk, J. Phys. Chem. C, 114, 2208–2219, doi:10.1021/jp909535c, 2010b.

Kim, S., Huey, L. G., Stickel, R. E., Tanner, D. J., Crawford, J. H., Olson, J. R., Chen, G., Brune, W. H., Ren, X., Lesher, R., Wooldridge, P. J., Bertram, T. H., Perring, A., Cohen, R. C., Lefer, B. L., Shetter, R. E., Avery, M., Diskin, G., and Sokolik, I.: Measurement of HO_2NO_2 in the free troposphere during the intercontinental chemical transport experiment – North America 2004, J. Geophys. Res.-Atmos., 112, D12S01, doi:10.1029/2006JD007676, 2007.

Kleffmann, J., Heland, J., Kurtenbach, R., Lorzer, J., and Wiesen, P.: A new instrument (LOPAP) for the detection of nitrous acid (HONO), Environ. Sci. Pollut. Res., 48–54, 2002.

Knight, G., Ravishankara, A. R., and Burkholder, J. B.: UV absorption cross sections of HO_2NO_2 between 343 and 273 K, Phys. Chem. Chem. Phys., 4, 1432–1437, doi:10.1039/b108904h, 2002.

Krepelova, A., Newberg, J. T., Huthwelker, T., Bluhm, H., and Ammann, M.: The nature of nitrate at the ice surface studied by XPS and NEXAFS, Phys. Chem. Chem. Phys., 12, 8870–8880, doi:10.1039/c0cp00359j, 2010.

Lammel, G., Perner, D., and Warneck, P.: Decomposition of pernitric acid in aqueous-solution, J. Phys. Chem.-US, 94, 6141–6144, 10.1021/j100378a091, 1990.

Lelieveld, J. and Crutzen, P. J.: The role of clouds in tropospheric photochemistry, J. Atmos. Chem., 12, 229–267, doi:10.1007/BF00048075, 1991.

Li, Z. J., Friedl, R. R., Moore, S. B., and Sander, S. P.: Interaction of peroxynitric acid with solid H_2O ice, J. Geophys. Res.-Atmos., 101, 6795–6802, doi:10.1029/96JD00065, 1996.

Liss, P. S. and Slater, P. G.: Flux of gases across air-sea interface, Nature, 247, 181–184, doi:10.1038/247181a0, 1974.

Longfellow, C. A., Imamura, T., Ravishankara, A. R., and Hanson, D. R.: HONO solubility and heterogeneous reactivity on sulfuric acid surfaces, J. Phys. Chem. A, 102, 3323–3332, doi:10.1021/jp9807120, 1998.

Marsh, A. R. W. and McElroy, W. J.: The dissociation-constant and Henry law constant of HCl in aqueous-solution, Atmos. Envrion., 19, 1075–1080, doi:10.1016/0004-6981(85)90192-1, 1985.

McNeill, V. F., Loerting, T., Geiger, F. M., Trout, B. L., and Molina, M. J.: Hydrogen chloride-induced surface disordering on ice, P. Nat. Acad. Sci. USA, 103, 9422–9427, doi:10.1073/pnas.0603494103, 2006.

McNeill, V. F., Geiger, F. M., Loerting, T., Trout, B. L., Molina, L. T., and Molina, M. J.: Interaction of hydrogen chloride with ice surfaces: The effects of grain size, surface roughness, and surface disorder, J. Phys. Chem. A, 111, 6274–6284, doi:10.1021/jp068914g, 2007.

Niki, H., Maker, P. D., Savage, C. M., and Breitenbach, L. P.: Fourier-transform IR spectroscopic observation of pernitric acid formed via HOO + $NO_2 -> HOONO_2$, Chem. Phys. Lett., 45, 564–566, doi:10.1016/0009-2614(79)85027-7, 1977.

Peybernes, N., Marchand, C., Le Calve, S., and Mirabel, P.: Adsorption studies of acetone and 2,3-butanedione on ice surfaces between 193 and 223 K, Phys. Chem. Chem. Phys., 6, 1277–1284, doi:10.1039/b315064j, 2004.

Picaud, S., Hoang, P. N. M., Peybernes, N., Le Calve, S., and Mirabel, P.: Adsorption of acetic acid on ice: Experiments and molecular dynamics simulations, J. Chem. Phys., 122, 194707, doi:10.1063/1.1888368, 2005.

Popp, P. J., Gao, R. S., Marcy, T. P., Fahey, D. W., Hudson, P. K., Thompson, T. L., Karcher, B., Ridley, B. A., Weinheimer, A. J., Knapp, D. J., Montzka, D. D., Baumgardner, D., Garrett, T. J., Weinstock, E. M., Smith, J. B., Sayres, D. S., Pittman, J. V., Dhaniyala, S., Bui, T. P., and Mahoney, M. J.: Nitric acid uptake on subtropical cirrus cloud particles, J. Geophys. Res.-Atmos., 109, D06302, doi:10.1029/2003JD004255, 2004.

Possanzini, M., Dipalo, V., and Liberti, A.: Annular denuder method for determination of H_2O_2 in the ambient atmosphere, Sci. Total Environ., 77, 203–214, doi:10.1016/0048-9697(88)90056-3, 1988.

Pouvesle, N., Kippenberger, M., Schuster, G., and Crowley, J. N.: The interaction of H_2O_2 with ice surfaces between 203 and 233 K, Phys. Chem. Chem. Phys., 12, 15544–15550, doi:10.1039/c0cp01656j, 2010.

Regimbal, J. M. and Mozurkewich, M.: Peroxynitric acid decay mechanisms and kinetics at low pH, J. Phys. Chem. A, 101, 8822–8829, doi:10.1021/jp971908n, 1997.

Servant, J., Kouadio, G., Cros, B., and Delmas, R.: Carboxylic monoacids in the air of mayombe forest (Congo) – Role of the forest as a source or sink, J. Atmos. Chem., 12, 367–380, doi:10.1007/BF00114774, 1991.

Slusher, D. L., Pitteri, S. J., Haman, B. J., Tanner, D. J., and Huey, L. G.: A chemical ionization technique for measurement of pernitric acid in the upper troposphere and the polar boundary layer, Geophys. Res. Lett., 28, 3875–3878, doi:10.1029/2001GL013443, 2001.

Slusher, D. L., Huey, L. G., Tanner, D. J., Chen, G., Davis, D. D., Buhr, M., Nowak, J. B., Eisele, F. L., Kosciuch, E., Mauldin, R. L., Lefer, B. L., Shetter, R. E., and Dibb, J. E.: Measurements of pernitric acid at the South Pole during ISCAT 2000, Geophys. Res. Lett., 29, 2011, doi:10.1029/2002GL015703, 2002.

Slusher, D. L., Neff, W. D., Kim, S., Huey, L. G., Wang, Y., Zeng, T., Tanner, D. J., Blake, D. R., Beyersdorf, A., Lefer, B. L., Crawford, J. H., Eisele, F. L., Mauldin, R. L., Kosciuch, E., Buhr, M. P., Wallace, H. W., and Davis, D. D.: Atmospheric chemistry results from the ANTCI 2005 Antarctic plateau airborne study, J. Geophys. Res.-Atmos., 115, D07304, doi:10.1029/2009JD012605, 2010.

Sokolov, O. and Abbatt, J. P. D.: Adsorption to ice of n-alcohols (ethanol to 1-hexanol), acetic acid, and hexanal, J. Phys. Chem. A, 106, 775–782, doi:10.1021/jp013291m, 2002.

Symington, A., Cox, R. A., and Fernandez, M. A.: Uptake of organic acids on ice surfaces: Evidence for surface modification and hydrate formation, Z. Phys. Chem., 224, 1219–1245, doi:10.1524/zpch.2010.6149, 2010.

Thibert, E. and Dominé, F.: Thermodynamics and kinetics of the solid solution of HNO_3 in ice, J. Phys. Chem. B, 102, 4432–4439, doi:10.1021/jp980569a, 1998.

Ullerstam, M., Thornberry, T., and Abbatt, J. P. D.: Uptake of gas-phase nitric acid to ice at low partial pressures: evidence for unsaturated surface coverage, Faraday Discuss., 130, 211–226, doi:10.1039/b417418f, 2005.

Vlasenko, A., Huthwelker, T., Gaggeler, H. W., and Ammann, M.: Kinetics of the heterogeneous reaction of nitric acid with mineral dust particles: An aerosol flowtube study, Phys. Chem. Chem. Phys., 11, 7921–7930, doi:10.1039/b904290n, 2009.

von Hessberg, P., Pouvesle, N., Winkler, A. K., Schuster, G., and Crowley, J. N.: Interaction of formic and acetic acid with ice surfaces between 187 and 227 K. Investigation of single species- and competitive adsorption, Phys. Chem. Chem. Phys., 10, 2345–2355, doi:10.1039/b800831k, 2008.

Wilhelm, E., Battino, R., and Wilcock, R. J.: Low-pressure solubility of gases in liquid water, Chem. Rev., 77, 219–262, doi:10.1021/cr60306a003, 1977.

Winkler, A. K., Holmes, N. S., and Crowley, J. N.: Interaction of methanol, acetone and formaldehyde with ice surfaces between 198 and 223 K, Phys. Chem. Chem. Phys., 4, 5270–5275, 2002.

Yaws, C. L. and Yang, H.-C.: Henry's law constant for compound in water, Thermodynamic and Physical Property Data, edited by: Yaws, C. L., Gulf Publishing Company, Houston, Texas, 1992.